An eco-friendly synthesis of ZnO nanoparticles with jamun seed extract and their multi-applications

ALQAHTANI, Mohammed S., SYED, Rabbani, SHAHID, Mudassar, ALRASHOUDI, Reem Hamoud, MATEEN, Ayesha, LAKSHMIPATHY, R. and GOEL, Mukesh <http://orcid.org/0000-0003-2991-3439>

Research Article

Mohammed S. Alqahtani, Rabbani Syed*, Mudassar Shahid, Reem Hamoud Alrashoudi, Ayesha Mateen, R. Lakshmipathy*, and Mukesh Goel

An eco-friendly synthesis of ZnO nanoparticles with jamun seed extract and their multi-applications

https://doi.org/10.1515/rams-2025-0134
received September 21, 2024; accepted July 14, 2025

Abstract: Zinc oxide (ZnO) nanoparticles were synthesized *via* an ecofriendly route using Indian Jamun seed aqueous extract. The synthesized ZnO nanoparticles were characterized for their surface properties using characterization techniques such as UV-Visible, FTIR, XRD, SEM, EDX, and TEM. The synthesized ZnO nanoparticles were found to be spherical with a size ≤1 nm, as evidenced from SEM and TEM investigations. The XRD patterns confirm the formation of the wurtzite phase of ZnO nanoparticles. The ZnO nanoparticles were later investigated for their ability to remediate Hg^{2+} ions from aqueous solutions. Response surface methodology was employed to optimize the independent variables, and optimal results were achieved at pH 6, 45 min of contact time, and an initial concentration of 100 mg·L^{-1} Hg^{2+} ions. The applicability of the developed model was supported by a *p*-value of <0.0001 being significant, and 11 out of 20 runs resulted in above 75% of removal efficiency. The loading capacity of the ZnO nanoparticles was calculated to be 122.7 mg·g^{-1}. The decolourization of methylene blue was achieved successfully with ZnO nanoparticles within 150 min. A moderate antimicrobial activity was exhibited by the ZnO nanoparticles synthesized in this study, with zones of inhibition of 15 and 14 mm for *Escherichia coli* and *Staphylococcus aureus,* respectively. The results conclude that the Indian jamun seed extract-mediated ZnO nanoparticles are excellent candidates for the remediation of Hg^{2+} ion-contaminated water streams.

Keywords: ZnO, Indian jamun seeds, green synthesis, mercury, adsorption

1 Introduction

Metal oxide nanoparticles have gained significant popularity in all domains of industrial applications. Their ability to exhibit excellent stability under higher pressure and temperature has attracted researchers to synthesize various metal oxide nanoparticles [1]. Zinc oxide (ZnO) nanoparticles have attained significance among the metal oxides due to their versatile applications, ranging from engineering to biology [2]. ZnO nanoparticles are used as sensors [3], photocatalysts [4], adsorbents [2], antimicrobials [5], antifungals [6], anticancers [7] antioxidants [8], and antiparasitic [9] agents. Various methods are in practice for the production of ZnO nanoparticles; however, the green synthesis of ZnO nanoparticles is found to be prolific due to ease and ecofriendliness [10]. Further, the cost of the synthesis is economical with minimal reagents and produces nanoparticles that contain biologically active molecules on its surface that can enhance the biological activities and adsorption process [2,5–8].

Literature reveals the use of several natural plants and fruit waste extracts for the prolific production of ZnO nanoparticles. Extracts of green tea were successfully used for the generation of ZnO nanoparticles, and the synthesized ZnO nanoparticles were successfully evaluated for their ability to sense gases [3]. *Origanum majorana* was employed for the synthesis of spherically shaped ZnO nanoparticles with negative charge [11]. The as-synthesized

* **Corresponding author: Rabbani Syed,** Department of Clinical Laboratory Sciences, College of Applied Medical Sciences, King Saud University, Riyadh, 11451, Saudi Arabia, e-mail: rsyed@ksu.edu.sa
* **Corresponding author: R. Lakshmipathy,** Directorate of Learning and Development, SRM Institute of Science and Technology, Kattankulathur, 603203, Chengalpattu, Tamil Nadu, India, e-mail: lakshmipathy.vit@gmail.com
Mohammed S. Alqahtani, Mudassar Shahid: Department of Clinical Laboratory Sciences, College of Applied Medical Sciences, King Saud University, Riyadh, 11451, Saudi Arabia
Reem Hamoud Alrashoudi, Ayesha Mateen: Department of Pharmaceutics, College of Pharmacy, King Saud University, P.O. Box 2457, Riyadh, 11451, Saudi Arabia
Mukesh Goel: Department of Engineering and Maths, College of Business, Technology and Engineering, Sheffield Hallam University, Sheffield, United Kingdom

nanoparticles exhibited less cytotoxicity against normal cells and anticancer activity. *Nauclea latifolia* fruit extract was used as a bioreductant and stabilizer for the synthesis of ZnO nanoparticles with a size of 12–17 nm [12]. The ZnO nanoparticles were applied in the adsorption of methyl green from aqueous solutions and were able to achieve 99.9% removal efficiency. *Acacia catechu* leaf extracts were utilized for the fabrication of ZnO nanoparticles, and ZnO was employed in the removal of arsenic from water [13]. Under optimal conditions, 90% removal efficiency of arsenic was achieved by the ZnO nanoparticles. *Rubia cordifolia* root extract-mediated synthesis of ZnO nanoparticles was reported, and the sizes of the ZnO nanoparticles were reported to be 17 nm [14]. They were applied in the sono-photocatalytic degradation of rhodamine B dye and assessed for their antibacterial activity. Leaf extracts of *Syzygium cumini* were employed in the generation of the ZnO nanoparticles, and the spherical nanoparticles were confirmed by the TEM technique [15]. Further, the nanoparticles were successfully employed in the photocatalytic degradation of methylene blue (MB) dye. Literature reveals that the plant and agro-wastes are prolific in the production of ZnO nanoparticles; however, the control of size and shape determines the type of application the ZnO nanoparticles exhibit, and it is essential to design a biological synthesis route toward the size and shape-controlled synthesis. In view of this, efforts were made in this study to explore the unexplored *Syzygium cumini* fruit seed extract as a potential source for the synthesis of ZnO nanoparticles.

Indian Jamun (*Syzygium cumini*) tree is native to the Indian subcontinent, and its fruits are consumed for their various medicinal values. The seeds of the jamun fruit are usually discarded as waste; however, the seeds are found to be rich in flavonoids, antioxidants, and proteins in addition to calcium [9,16]. The seeds of the jamun fruit have not been explored for the synthesis of zinc nanoparticles, and the objective of this investigation is to use jamun seed extracts for the synthesis of ZnO nanoparticles. The synthesized ZnO nanoparticles were explored for the adsorption of Hg^{2+} ions from aqueous solutions. Since Hg^{2+} ions are toxic and detrimental to aquatic ecosystems [17], they were selected as the target analyte in this study. In addition to the above, the photocatalytic ability of ZnO nanoparticles was explored toward MB cationic dye MB. Unlike other dyes, MB is extensively used in the textile and dyeing industries and is released abundantly into the water streams. Considering the potential impacts of MB, such as carcinogenic and degradation of water quality [18], it was chosen as a target analyte for the degradation studies. Further, the antimicrobial activity of the ZnO nanoparticles was evaluated against two pathogens, *Escherichia coli* and *Staphylococcus aureus,* and the results are reported.

2 Materials and methods

2.1 Preparation of jamun seed aqueous extract

The Indian jamun seeds were collected from the local fruit market and washed several times under running tap water. The water-washed seeds were dried in the sunlight for 7 days, and the shells of the seeds were removed. The shells removed seeds were powdered using a conventional mixture, and the powder was stored in air air-tight container for the preparation of aqueous extract. For preparation of the aqueous extract, 2 g of jamun seed powder was added to 100 mL of deionized water and heated at 65°C with constant stirring for 120 min [10]. The yellowish decoction obtained was filtered using Whatman filters, and the fresh aqueous extract was used for the synthesis of ZnO nanoparticles.

2.2 Preparation of ZnO nanoparticles

To prepare the ZnO nanoparticles, first, 0.1 M of zinc acetate solution was prepared, and to the 100 mL of 0.1 M solution, 10 mL of freshly prepared aqueous extract of Indian jamun seeds was added drop by drop with constant stirring. The addition of aqueous extract turned the solution pale yellow, and to this, 0.1 M NaOH was added drop by drop until the pH turned to 10. The mixture was stirred continuously, and the formation of white precipitate was observed. The white precipitate was separated by filtration and dried in an oven at 75°C for 180 min. The dried samples were stored for further characterization and application studies (Scheme 1).

2.3 Characterization techniques

The absorption bands of ZnO nanoparticles were investigated using a UV-visible spectrophotometer (Shimadzu, UV3600 Plus). The surface functional groups of ZnO nanoparticles were studied by FTIR spectroscopy (Shimadzu, IRtracer 100), and the sample was analyzed in ATR mode between 4,000 and 400 cm^{-1}. The diffraction patterns of ZnO nanoparticles were obtained using powder X-ray diffraction (PANalytical, Netherlands). The surface morphology was investigated by scanning electron microscopy (Supra 55 – Carl Zeiss, Germany). The size and shape morphology of ZnO were investigated using a transmission

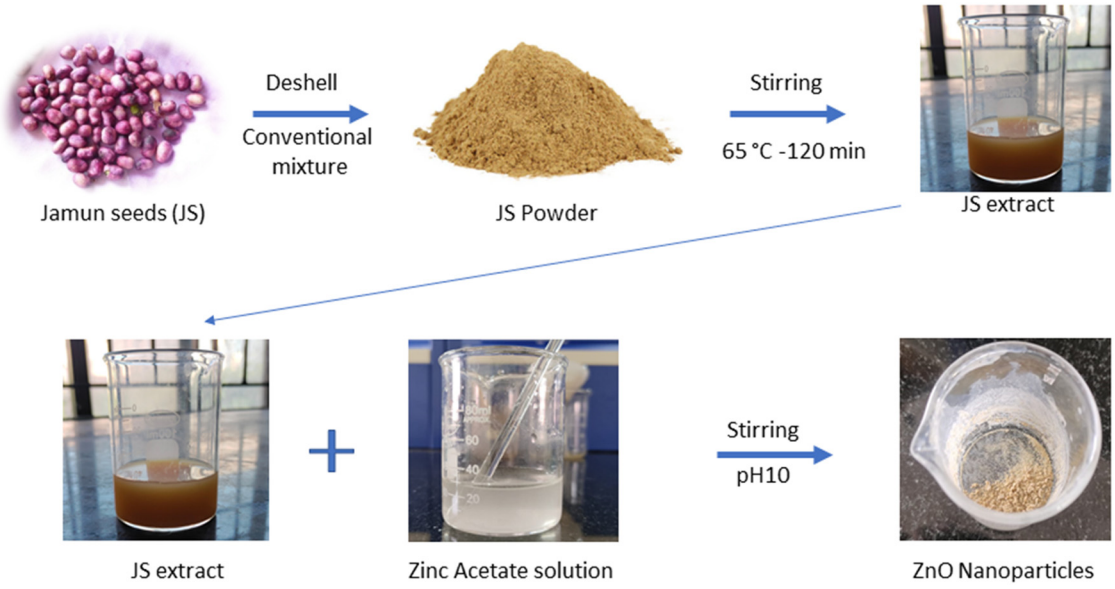

Scheme 1: Synthesis of ZnO nanoparticles using jamun seed aqueous extract.

electron microscope (G2-20 Twin, FEI Tecnai) operated at 200 kV. The residual concentration of Hg^{2+} ions was estimated using an atomic absorption spectrophotometer (AA240, Varian). The hollow cathode lamp was operated at 253.7 nm with acetylene, air, fuel, and oxidant.

2.4 Response surface methodology (RSM)

A popular method that is very commonly used in RSM is the central composite design (CCD). It is used to study how different factors affect metal adsorption. A key benefit of CCD is that it requires fewer experiments compared to other methods while still providing good results. This makes it efficient for fitting data and building models. In this research, a full factorial design with 20 experiments was used. The important factors and their details are provided in Table 1. The software Design Expert 13 was used to create the CCD.

Table 1: Optimization of independent variables, their levels, and symbols

Variables	Symbol	Levels		
		−1	0	+1
pH	A	4	6	8
Contact time	B	30	45	60
Initial concentration	C	50	100	150

2.5 Photocatalytic activity

The ability of ZnO nanoparticle synthesis by jamun seed extracts to potentially decolourize the MB cationic dye *via* photocatalytic activity was investigated. Investigations were performed by the addition of 0.1 g of ZnO nanoparticles to 100 mL of 100 mg·L^{-1} MB with stirring using a magnetic stirrer. The entire working solution was placed in a photoreactor equipped with a UV light source. Samples were drawn at 10 and 150 min time intervals, and the residual concentration of MB was tested with a UV-visible spectrophotometer. The MB residual concentrations in solution were determined using Eq. (1)

$$\% \text{ MB decolourized} = \frac{\text{MB}_0 - \text{MB}_t}{\text{MB}_0} \times 100, \quad (1)$$

where MB_0 is the initial MB concentration and MB_t is the final concentration.

2.6 Microbial growth and cultivation methods

Microbial cultures were grown on potato dextrose agar (PDA) plates and kept at 4°C, while the stock cultures were incubated in the dark at 25°C on PDA for 7 days. To prepare the growth medium, 80 g of glucose and 500 mL of fresh potato extract were combined with 3.5 L of distilled water. The potato extract was made by dicing 1 kg of potatoes and boiling them in 2 L of distilled water for 30 min.

The medium was then portioned into 350 mL beakers, with each receiving 50 mL, and sterilized by autoclaving at 121°C for 30 min. Fresh microbial samples, grown on PDA plates for 7 days at 28°C, were used to inoculate vials. After a 10-day incubation at 25°C, the cultures were filtered using filter paper to separate the filtrate from the mycelium. The filtrate was mixed with ethyl acetate and shaken at 250 rpm for 20 min at room temperature. The mixture was then filtered, and the extract was concentrated using a rotary evaporator under vacuum at 40°C, producing 2 g of a brown product.

2.7 Antimicrobial assay

The antibacterial activity of the ZnO nanoparticles was evaluated using the standard agar well diffusion method on Mueller–Hinton agar (MHA) medium. MHA plates were prepared by pouring the sterilized medium into sterile Petri dishes under aseptic conditions and allowed to solidify for 1 h at room temperature. Overnight bacterial cultures of *E. coli* (Gram-negative) and *S. aureus* (Gram-positive) were adjusted to a concentration of approximately 10^8 CFU·mL^{-1} (0.5 McFarland standard) and uniformly spread across the surface of the MHA plates using a sterile cotton swab. Sterile wells of 7–8 mm diameter were carefully punched into the agar using a sterile cork borer. The ZnO nanoparticle suspensions were prepared in sterile distilled water, and 50 µL of the suspension was pipetted into the respective wells. Plates were pre-incubated at room temperature for 30 min to facilitate the diffusion of the test samples into the agar. Subsequently, the plates were incubated at 37°C for 24 h to allow bacterial growth and interaction with the ZnO nanoparticles. Following incubation, zones of inhibition (ZOIs) were measured using a calibrated ruler to assess the antibacterial activity. The ZOI around the wells indicated the efficacy of the ZnO nanoparticles against the test bacterial strains. All experiments were performed in triplicate to ensure reproducibility and statistical significance.

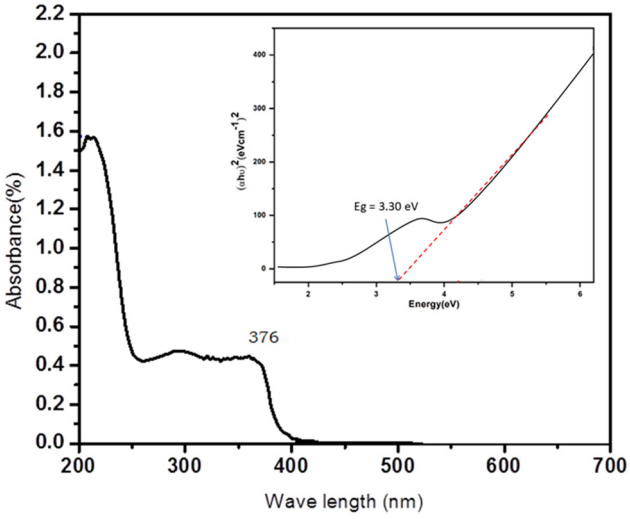

Figure 1: UV-Visible spectra of ZnO nanoparticles synthesized using Indian jamun seed extracts.

3 Results and discussion

3.1 UV-Visible spectroscopy

The initial confirmation of the formation of ZnO nanoparticles was performed with UV-Visible spectral analysis, and the results are displayed in Figure 1. Peaks between 200

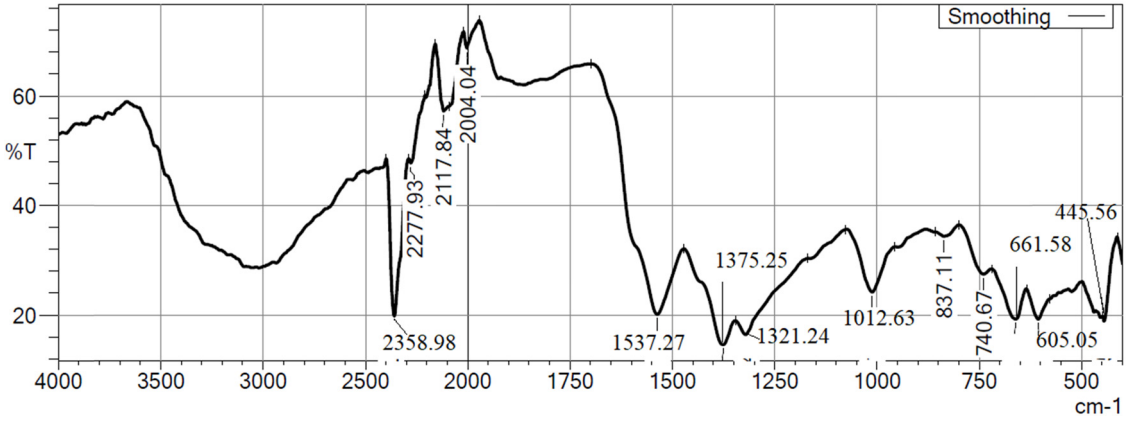

Figure 2: FTIR spectra of ZnO nanoparticles synthesized using Indian jamun seed extract.

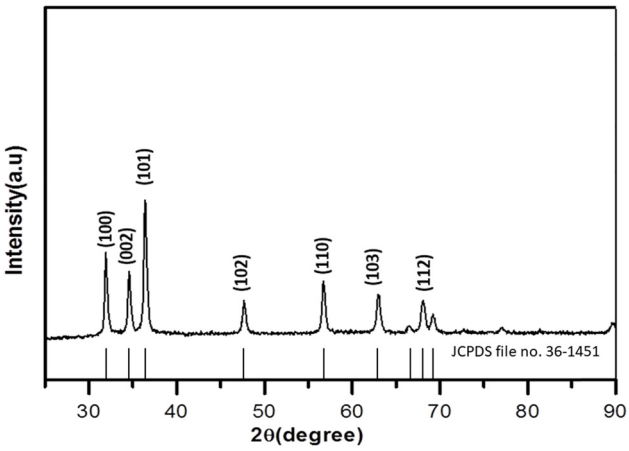

Figure 3: Patterns of X-ray diffraction obtained for the ZnO nanoparticles synthesized using jamun seed extract.

and 300 nm are due to the presence of organic molecules that were capping the ZnO nanoparticles. A maximum absorption peak at 376 nm observed in the spectra confirms the formation of ZnO nanoparticles that arise due to an electron transition from the valence band to the conduction band.

The band gap of the ZnO nanoparticles was calculated applying the Tauc's relation on the absorbance as follows [19]:

$$(\alpha h\nu)^{\frac{1}{n}} = B(h\nu - E_g), \tag{2}$$

where α is the molar extinction coefficient, h is Planck's constant, ν represents the frequency, B is a constant, and n is a factor that depends on the type of electron transition.

A band gap of 3.30 eV was calculated for the ZnO nanoparticles synthesized in this study using the plot of $(\alpha h\nu)^2$

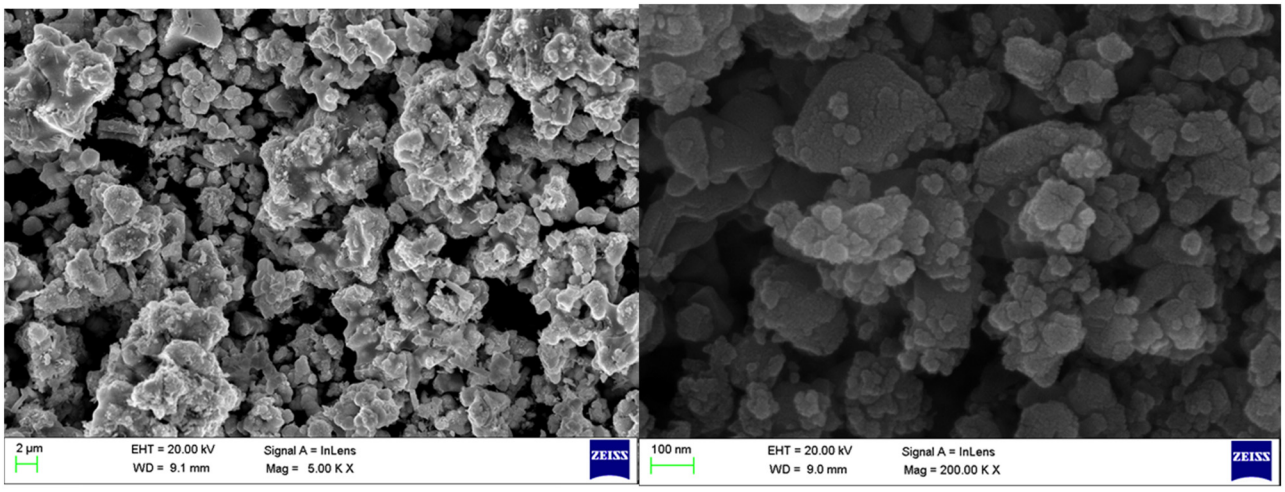

Figure 4: SEM images of ZnO nanoparticles synthesized using jamun seed extract.

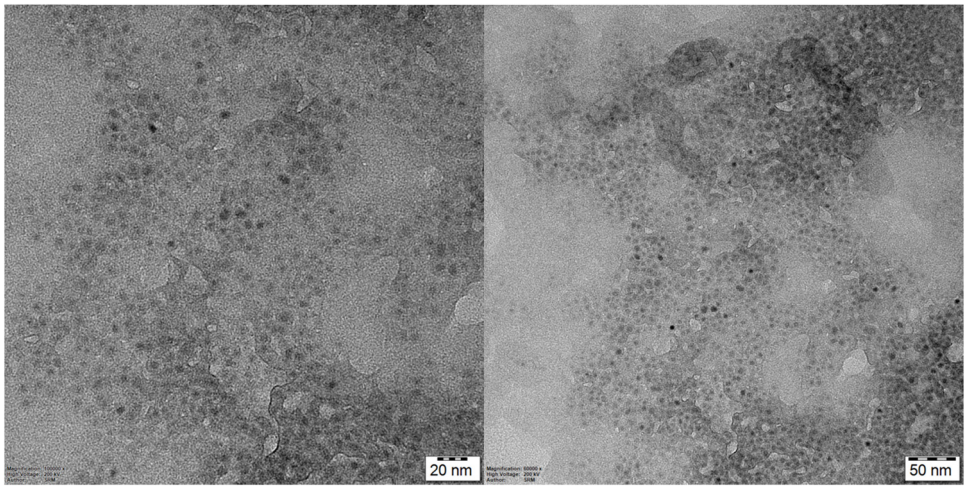

Figure 5: TEM images of ZnO nanoparticles synthesized using jamun seed extract.

vs hv as shown in the inset of Figure 1. The high band gap can be effective in photocatalytic applications. This is in good agreement with the literature for the green synthesis of ZnO nanoparticles using natural plant extracts [20,21].

3.2 FTIR spectroscopy

The ZnO nanoparticles were subjected to FTIR spectroscopy and displayed several absorption bands corresponding to various functional groups (Figure 2). The strong and broad absorption intensity at 3,094 cm^{-1} corresponds to the stretching vibrations of the −OH groups of bioactive molecules such as alcohols and phenols from the seed aqueous extract [22]. The bands at 2,117 and 2,004 cm^{-1} correspond to the stretching vibrations of nitriles and cumulative double bonds of the metal carbonyl complex. A peak at 1,537 cm^{-1} is due to the stretching vibrations of C═C groups. The bands between 1,321 and 1,012 cm^{-1} correspond to the complementary stretching bands of the C−O groups of biomolecules [23]. The bands between 740 and 605 cm^{-1} are overtones of nitrile vibrations. A peak at 445 cm^{-1} confirms the

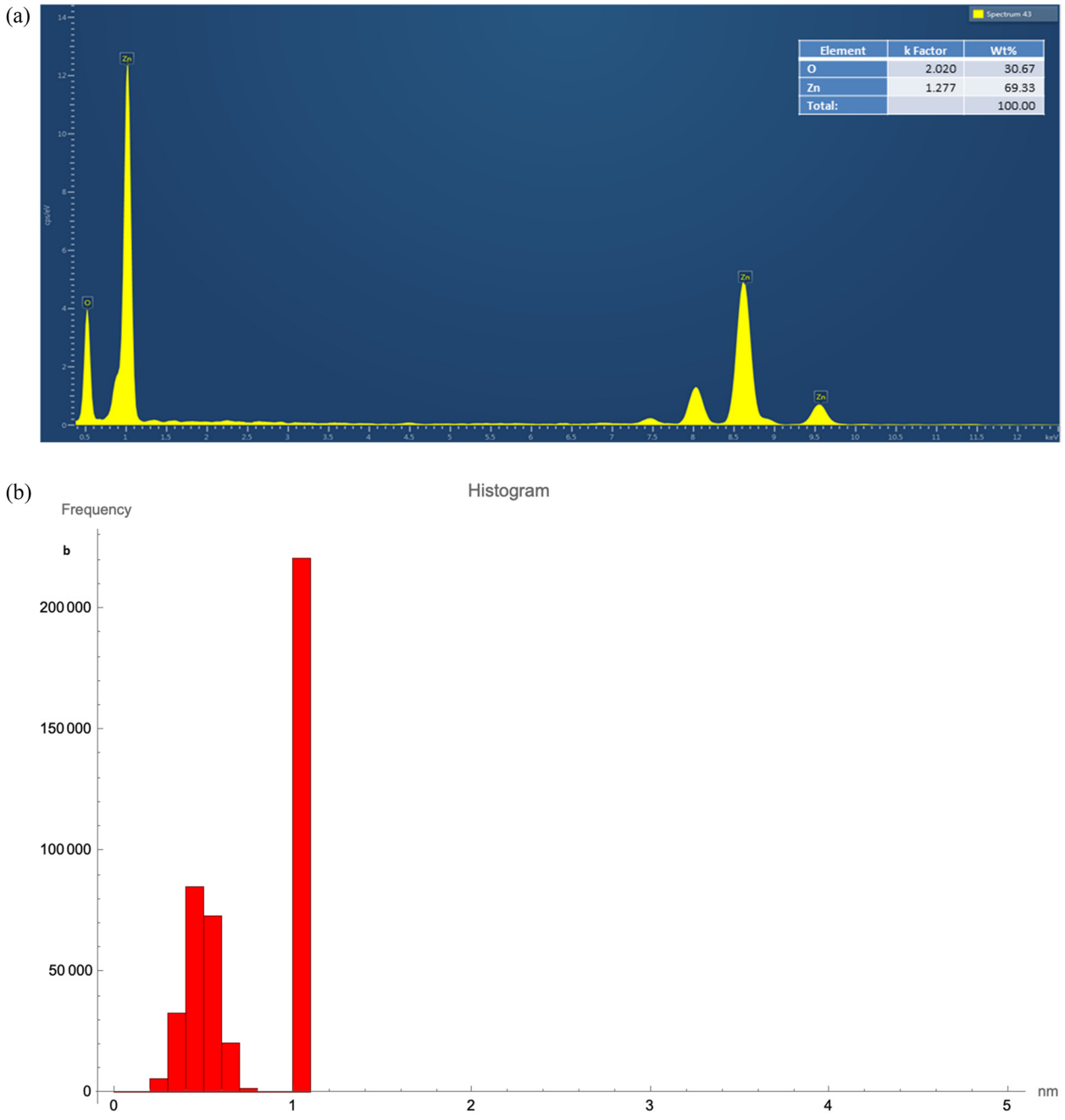

Figure 6: (a) EDX pattern of ZnO nanoparticles synthesized using jamun seed extract and (b) histogram obtained from the TEM image.

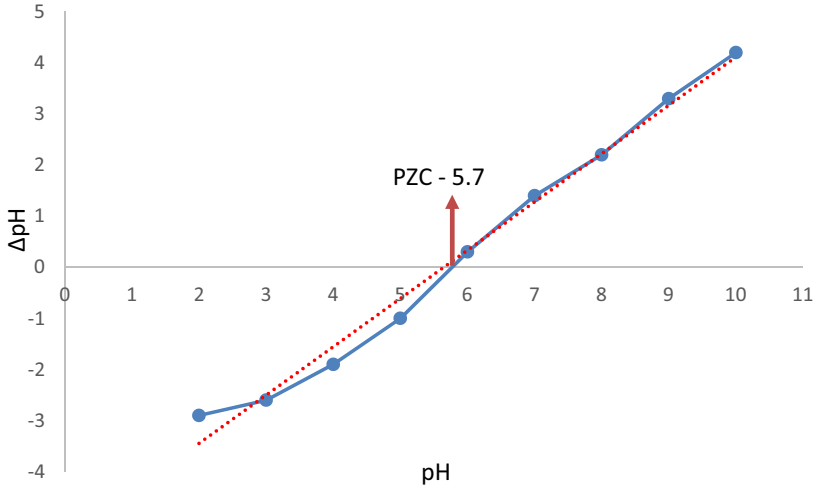

Figure 7: Plot determining the pH_{pzc} of the ZnO nanoparticles.

presence of ZnO that are attributed to the Zn–O bond vibrations [24]. The presence of functional groups in the FTIR spectra confirms that the biomolecules of the jamun seed extract stabilized the ZnO nanoparticles.

3.3 XRD

The diffraction patterns of ZnO nanoparticles were recorded with the XRD technique, and the results are presented in Figure 3. The XRD patterns displayed well-crystalline ZnO peaks, corresponding to the hexagonal wurtzite structure. The presence of crystalline peaks at the (100), (002), (101), (102), (110), (103), and (112) planes reveals the hcp wurtzite structure and matches the JCPDS file no. 036-1451. Similar patterns were obtained for the ZnO nanoparticles synthesized using the stem extract of *Swertia chirayita* [25]. The sharp and well-defined peaks in the X-ray diffraction pattern show that the sample is very pure and has a highly ordered crystal structure. The broadening of the peaks and Scherrer's equation are used to estimate the average size of the tiny

Table 2: CCD runs and comparison of experimental and predicted values for the removal of Hg^{2+} ions by ZnO nanoparticles

		Factor 1	Factor 2	Factor 3	Removal (%)	
Std	Run	A: pH	B: Contact time (min)	C: Initial concentration ($mg \cdot L^{-1}$)	Experimental	Predicted
17	1	6	45	100	81.2	81.32
2	2	8	30	50	77.6	75.75
13	3	6	45	15	91.3	89.93
4	4	8	60	50	72.1	78.37
6	5	8	30	150	42.3	48.68
11	6	6	20	100	59.5	57.94
18	7	6	45	100	81.3	81.32
1	8	4	30	50	30.8	35.00
15	9	6	45	100	81.3	81.32
5	10	4	30	150	36.4	30.79
20	11	6	45	100	81.2	81.32
10	12	9	45	100	51.3	46.76
16	13	6	45	100	81.3	81.32
14	14	6	45	180	81.2	81.71
9	15	3	45	100	9.5	12.87
19	16	6	45	100	81.3	81.32
3	17	4	60	50	56.8	51.07
8	18	8	60	150	76.8	73.26
7	19	4	60	150	66.3	68.81
12	20	6	70	100	91.2	91.81

crystal domains within the material [26]. The Scherrer equation is expressed as follows:

$$D = \frac{K\lambda}{(\beta \text{ Cos } \theta)}. \quad (3)$$

The crystal sizes of the ZnO nanoparticles synthesized using jamun seed extracts were estimated to be in the range of 5–22 nm under our experimental conditions.

3.4 Morphology investigations

The ZnO nanoparticles were investigated using a scanning electron microscope for surface morphology, and the results are depicted in Figure 4. The images revealed the nanosized ZnO particles that are uniformly distributed without any agglomerations. Further, the shapes were found to be spherical, which are distinctly visible in the images. The shape and size of the ZnO nanoparticles were visualized with a transmission electron microscope, and the images are represented in Figure 5. The images revealed the distinct spherical nanoparticles with a size <5 nm. The ZnO nanoparticles were uniformly distributed without agglomeration. The histogram obtained from the TEM image depicts the particle sizes being ≤1, suggesting the formation of ZnO nanoclusters and sub-nanoclusters (Figure 6b). A single major peak at 1 nm suggests the dominance of the nanocluster formation. Similar observations were reported for the synthesis of ZnO nanoparticles using *Aspalathus linearis* extract [27]. Energy dispersive X-ray was employed to profile the elements of the ZnO nanoparticles, and the EDX pattern is displayed in Figure 6a. It is clearly visible that the patterns depict only peaks of Zn and O atoms, and this confirms the absence of other elements and highlights the purity of the ZnO nanoparticles.

Table 3: ANOVA of Hg^{2+} ions removal by jamun seed extract-mediated ZnO nanoparticles

Source	Sum of squares	df	Mean square	*F*-value	*p*-value
Model	9178.31	9	1019.81	46.10	<0.0001
A: pH	1595.00	1	1595.00	72.11	<0.0001
B: Contact time	1399.46	1	1399.46	63.27	<0.0001
C: Initial concentration	72.82	1	72.82	3.29	0.0997
AB	90.45	1	90.45	4.09	0.0707
AC	261.06	1	261.06	11.80	0.0064
BC	240.90	1	240.90	10.89	0.0080
A^2	5388.95	1	5388.95	243.62	<0.0001
B^2	76.14	1	76.14	3.44	0.0932
C^2	35.48	1	35.48	1.60	0.2340
Residual	221.20	10	22.12		
Lack of fit	221.19	5	44.24	3.87	0.5633
Pure error	0.0133	5	0.0027		
Cor total	9399.51	19			
R^2	0.9765		Predicted R^2	0.7824	
Adjusted R^2	0.9553		Adeq precision	23.7367	

3.5 Point zero charge (PZC) of the ZnO nanoparticles

The PZC of ZnO nanoparticles was determined by the addition of ZnO nanoparticles to a series of solutions with varying pH from 2 to 10. The mixture was agitated for 12 h in an orbital shaker at 30°C and the solution pH was measured. A plot of pH *vs* ΔpH ($pH_{initial} - pH_{final}$) was plotted to determine the pH_{pzc} of the ZnO nanoparticles, as shown in Figure 7. It was observed that the pH_{pzc} of the ZnO nanoparticles was found to be around pH 5.7. The surface charge of the ZnO nanoparticles above the PZC will be negative, and it can attract the positively charged Hg^{2+} ions for binding onto the surface.

3.6 RSM-based optimization

To optimize the removal of Hg^{2+} ions by ZnO nanoparticles, a CCD was employed. Three independent variables, pH, contact time, and initial Hg^{2+} concentration, were chosen for investigation. The CCD comprised 20 runs, incorporating 6 axial and central points, along with 8 cubic points positioned within the design space. Tables 2 and 3 present the predicted and experimental design matrices, along with the analysis of variance (ANOVA) for this Hg^{2+} removal process. Design Expert 13 software was used to establish a quadratic model, resulting in a second-order polynomial equation (Eq. (4)) that expresses the relationship between these factors and Hg^{2+} removal efficiency:

$$\begin{aligned} \%\text{ Removal} = {} & 81.32 + 11.3\ A + 10.16\ B - 2.33\ C \\ & - 22.89\ A^2 - 2.32\ B^2 - 1.61\ C^2 - 3.36\ AB \\ & - 5.71\ AC + 5.49\ BC. \end{aligned} \quad (4)$$

The strengths of each factor (pH, contact time, concentration) on Hg^{2+} removal by ZnO nanoparticles can be determined by the coefficients in the quadratic equation (Eq. (2)). Positive coefficients mean a higher factor level and lead to better removal, while negative coefficients

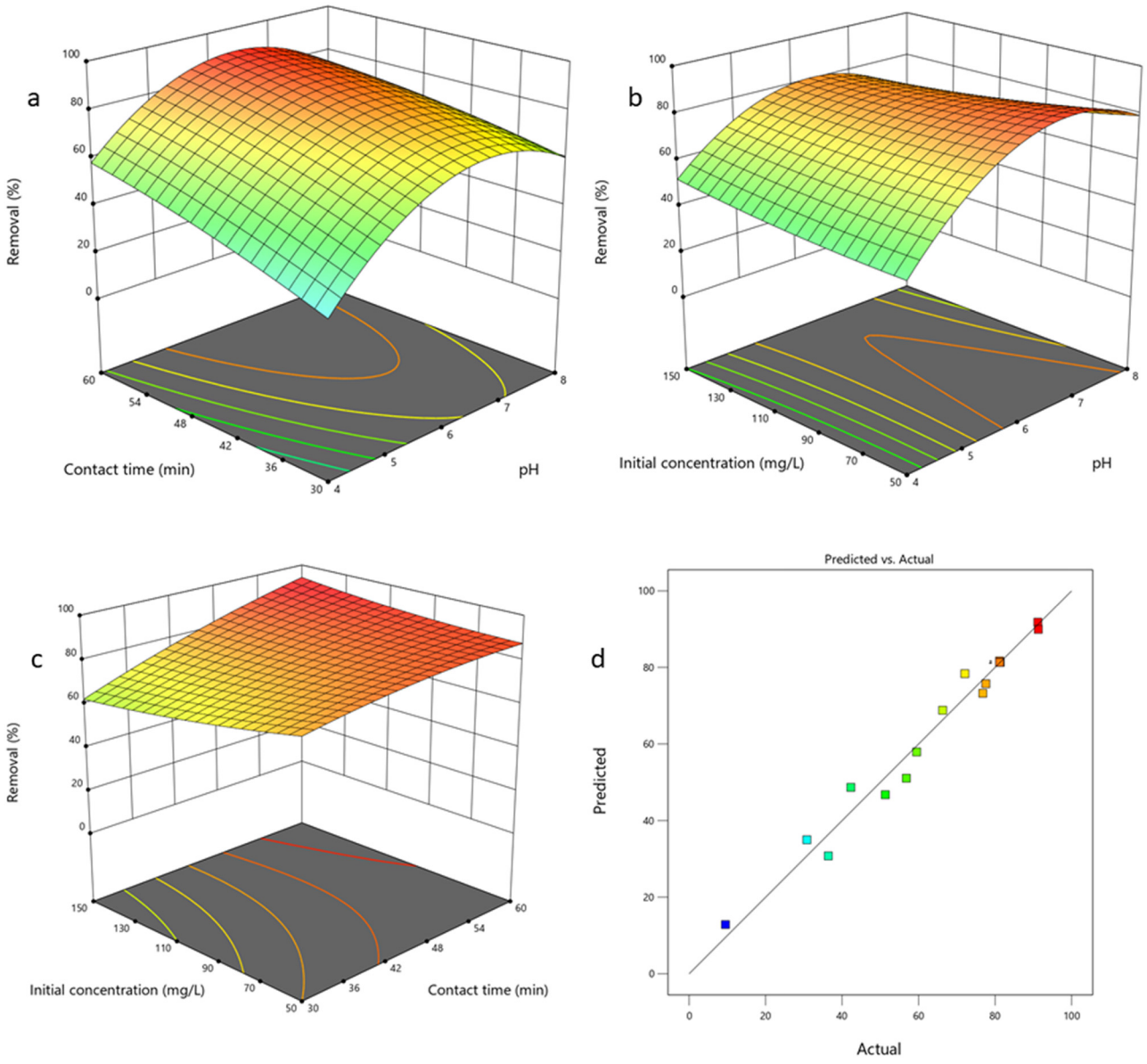

Figure 8: 3D surface plots for the removal of Hg^{2+} ions by ZnO nanoparticles: (a) pH *vs* contact time, (b) pH *vs* initial concentration, (c) contact time *vs* initial concentration, and (d) predicted *vs* actual plot.

indicate the opposite [28]. The equation also considers interactions between factors (two-factor terms) and how these interactions affect removal efficiency (curvature terms). The good agreement between predicted and experimental results (Table 2) validates the chosen model and suggests that the experiments achieved improved Hg^{2+} removal.

The ANOVA in Table 3 confirms the strength of the model for predicting Hg^{2+} removal by ZnO nanoparticles. An incredibly small *p*-value (<0.0001) indicates statistical significance, meaning that the model is unlikely due to random chance. High *F*-value (46.10) further supports the model's reliability. Larger *F*-values indicate a lower probability (0.01%) that the results occurred by chance [29]. Additionally, a lack-of-fit *F*-value greater than 0.1 suggests the absence of unexplained variations in this model. To ensure accuracy, it was examined how well the predicted values matched the actual results. Figure 8d displays this analysis, with points scattered randomly along a straight line. This indicates a normal data distribution without any significant deviations. This eliminates the need for data transformation and confirms the model's validity. Finally, correlation coefficients close to 1 (0.976) and high adjusted and predicted *R*-squared values (0.955 and 0.782,

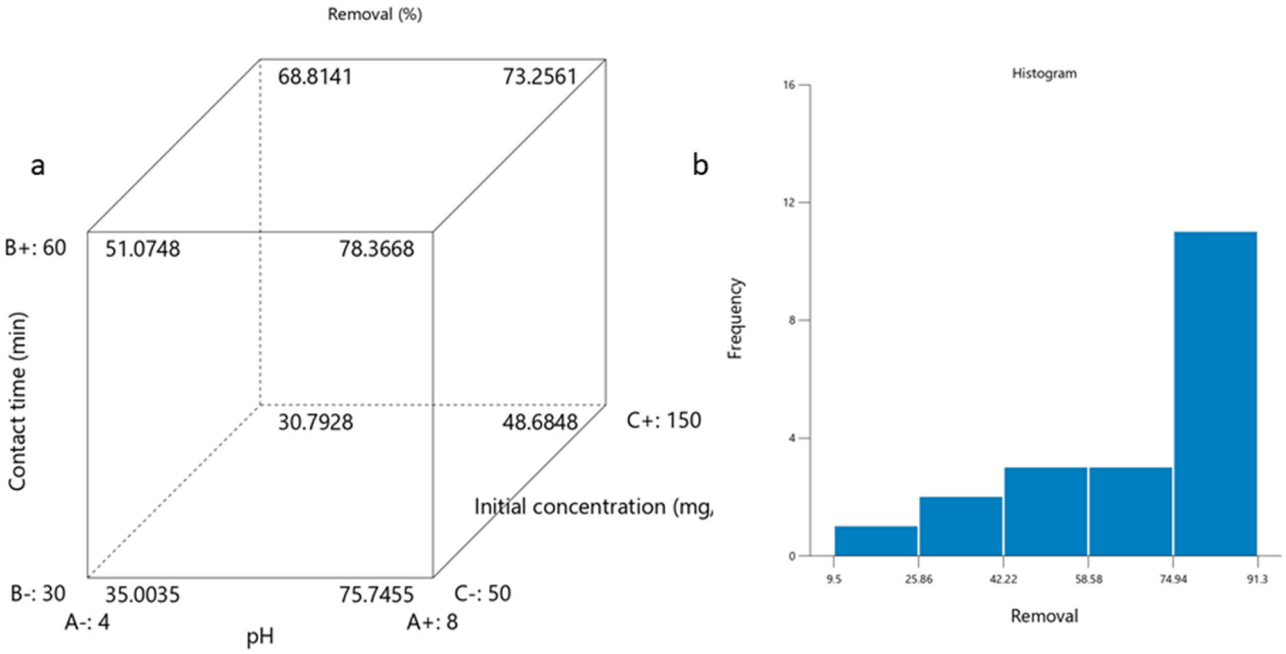

Figure 9: (a) Percentage removal at minimum and maximum points of independent variables and (b) histogram of frequency of percentage removal for the removal of Hg^{2+} ions by ZnO nanoparticles.

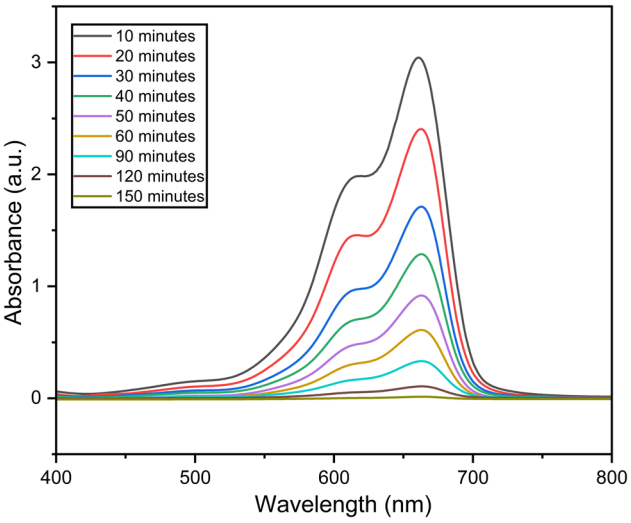

Figure 10: Photocatalytic decolourization of MB by ZnO nanoparticles synthesized using jamun seed extract.

respectively) further support the model's applicability. An adequate precision value of 23.7 signifies that the model has strong signals for accurate predictions.

The visualization of independent variables interacting with each other and their effect on the elimination of Hg^{2+} ions by ZnO nanoparticles was obtained by 3D surface plots. The surface 3D plots obtained in this study, which provide crucial information, are presented in Figure 8. The interaction of independent variables pH and contact time and their effect on the elimination of Hg^{2+} ions is depicted in Figure 8a. It can be seen that with increasing pH and contact time, the removal efficiency increased and was found to be maximum at pH 6; this was supported by the pH_{pzc} being at pH 5.7. Further increase in the pH beyond 6 reduces the removal efficiency even at higher contact times, and this is due to the formation of several precipitating hydroxides. At low pH, the hydronium ions exhibit competitive adsorption for the surface-active sites, and thus, the removal efficiency is low. With a further increase in pH, the competitive adsorption exhibited by hydronium ions declines, and Hg^{2+} ion adsorption improves. The increase in removal efficiency with an increase in contact time is due to the availability of time for the Hg^{2+} ions to interact with the surface of the ZnO nanoparticles. The 3D surface plot depicts that both pH and contact time influence the % removal. The interaction of independent variables, pH and initial concentration, and their effect is depicted in Figure 8b. The efficiency of removal is found to increase up to 100 $mg{\cdot}L^{-1}$ of initial concentration and decreases with further increase in the initial concentration at optimal pH 6. With an increase in the initial concentration, the availability of the surface active sites on ZnO nanoparticles disappears due to occupancy, and thus the % removal declines. In the case of initial concentration and contact time, the synergistic influence of the independent variables on the removal percentage of Hg^{2+} ions is shown in Figure 8c. It was observed that with an increase in the

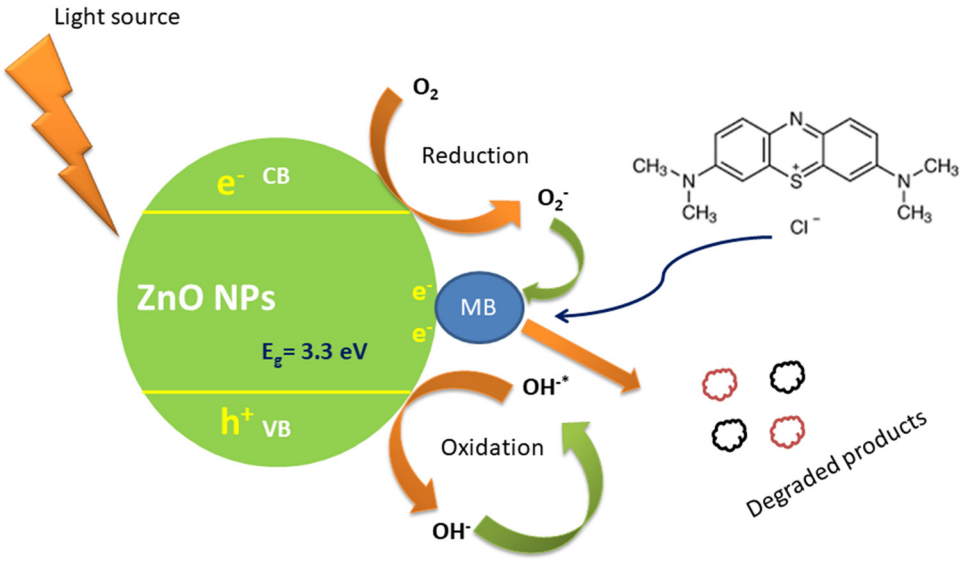

Figure 11: Mechanism of ZnO nanoparticles synthesized using jamun seed extract decolourizing MB ions.

contact time, the removal efficiency increases, and with increasing initial concentration, the efficiency decreases.

A 3D visualization of three independent variables and their % removal at minimum and maximum points is shown in Figure 9a, and a histogram of removal efficiency percentage for 20 runs is depicted in Figure 9b. It is seen that the frequency of % removal being greater than 75% is high compared to lower values. This indicates that the optimal values of independent variables, pH 6, contact time of 45 min, and initial concentration of 100 $mg{\cdot}L^{-1,}$ cause maximum removal of Hg^{2+} ions from aqueous solution by ZnO nanoparticles. The loading capacity of the ZnO nanoparticles was found to be 122.7 $mg{\cdot}g^{-1}$ toward Hg^{2+} ions. The higher loading observed in this study is due to the nanoclusters of ZnO nanoparticles providing a higher surface area for enhanced adsorption of Hg^{2+} ions.

Table 4: Photocatalytic activity comparison for the degradation of MB

S. no.	Catalyst	% Degradation	Time (min)	References
1	Ag nanoparticles	90	105	[31]
2	CuO nanostructures	83.5	120	[32]
3	Ni-doped CdS	91.3	240	[33]
4	Carbon-doped TiO_2	53	90	[34]
5	Nb-doped Fe_2O_3	87	120	[35]
6	ZnO nanoparticles	98	150	This study

3.7 Photocatalytic analysis

Figure 10 shows how a solution of MB loses its color over time when treated with ZnO nanoparticles made from jamun seed extract. The MB solution has a peak intensity at 665 nm, which weakens as time progresses. This weakening intensity reflects a decrease in MB concentration. In fact, the intensity at 665 nm nearly vanishes after 150 min. This disappearance indicates that the ZnO nanoparticles have decolorized MB, achieving a degradation efficiency of 98%. The ZnO nanoparticles' effectiveness in this photocatalytic process stems from two key properties: their large surface area due to small particle size nanoclusters, as evidenced in the TEM histogram, and their wide band gap that allows them to absorb a broader range of wavelengths [30]. Additionally, as previously established, ZnO nanoparticles can effectively adsorb cations onto their surface. In this case, the adsorption of MB cations by the ZnO nanoparticles facilitates their degradation. A more detailed explanation of this degradation mechanism is shown in Figure 11. A comparative table of photocatalytic activity of ZnO nanoparticles with other photocatalysts is summarized in Table 4, and it is noticed that the degradation

Table 5: Antimicrobial activity ZOI of species against ZnO nanoparticles

Species	ZOI (mm)
E. coli	15
S. aureus	14
Streptomycin disc	21

efficiency is high compared to several other photocatalysts reported in the literature.

3.8 Antimicrobial activity

The antimicrobial assay of ZnO nanoparticles synthesized using jamun seeds extract was tested against *E. coli* and *S. aureus,* and the results are presented in Table 5. The results displayed that the ZnO nanoparticles exhibit moderate antimicrobial activity against *E. coli* and *S. aureus,* respectively, compared to the standard streptomycin. The moderate activity exhibited by ZnO nanoparticles against both the species is due to the interaction of nanoparticles with the cell membranes of microbes, and thus disrupting the membranes, resulting in the leak of contents. In general, ZnO nanoparticles are known to be potential antimicrobial agents; however, in this study, it is found to be moderate, and this is due to the capping agents from jamun seeds hindering the interaction with the cell membranes of the microbial species. As a result, cell disruptions are not extensive, resulting in the moderate antimicrobial activity [36]. The antimicrobial activity of ZnO nanoparticles synthesized using Jamun seed extract is driven by various mechanisms. Nanoparticles physically damage bacterial membranes due to their nanoscale size and high surface energy, leading to the leakage of cellular contents and compromised membrane integrity. Second, ZnO nanoparticles generate reactive oxygen species such as hydroxyl radicals ($^{\cdot}OH$) and superoxide anions ($O_2^{\cdot-}$), which induce oxidative stress, damaging proteins, lipids, and DNA, ultimately impairing bacterial survival [37]. The release of Zn^{2+} ions disrupts bacterial enzymatic processes and interacts with thiol groups in proteins, further contributing to cell death [36].

4 Conclusion

The use of jamun seed extract for the successful synthesis of ZnO nanoparticles was demonstrated in this study. The synthesized ZnO nanoparticles were spherically shaped with a size ≤1 nm, and the wurtzite structure was confirmed using analytical techniques. The elemental analysis confirmed the purity of the formed ZnO nanoparticles, and optical investigations confirmed a 3.3 eV band gap. The adsorption experiments designed using RSM proved to be prolific for the removal of Hg^{2+} ions by ZnO nanoparticles. The significance of the developed model is well supported by the *p*-value <0.001 and higher *F*-value, and the predicted values coincide with the experimental values. In addition, 11 out of 20 runs exhibited greater than 75% of removal efficiency. The loading capacity was calculated to be 122.7 $mg \cdot g^{-1}$ under optimal conditions for Hg^{2+} ions by ZnO nanoparticles, which is noted to be competitive compared to various adsorbents. Further, the decolourization of MB was tested and evaluated with ZnO nanoparticles, and 98% of degradation efficiency was achieved within 150 min. The ZnO nanoparticles were moderately disrupting the cell membranes of *E. coli* and *S. aureus* with ZOI of 15 and 14 mm, thus exhibiting moderate antimicrobial activity. However, the standard disc exhibited higher inhibition, and further experiments are in progress to enhance the antimicrobial activity. The results project the ability of ZnO nanoparticles synthesized using Indian jamun seed extract to effectively adsorb Hg^{2+} ions and efficiently degrade MB from aqueous solution and further disrupt microbes' cell membranes.

Acknowledgments: The authors acknowledge and extend their appreciation to the Ongoing Research Funding Program (ORF-2025-739), King Saud University, Riyadh, Saudi Arabia, for funding this study. For the purpose of open access, the author has applied a Creative Commons Attribution (CC-BY) license to any Author Accepted Manuscript version of this paper arising from this submission.

Funding information: This study was funded by the Ongoing Research Funding Program (ORF-2025-739), King Saud University, Riyadh,Saudi Arabia.

Author contributions: MSA: investigation and data analysis; RS: conceptualization, project management, and formal analysis; MS: investigation and manuscript writing; RHA: investigation, software, and manuscript writing; AM: data analysis and resource management; RL: conceptualization, manuscript editing, and critical revision; and MG: manuscript review and editing and critical revision. All authors have accepted responsibility for the entire content of this manuscript and approved its submission.

Conflict of interest: The authors state no conflict of interest.

Data availability statement: All data generated or analyzed during this study are included in this published article.

References

[1] Aigbe, U. O. and O. A. Osibote. Green synthesis of metal oxide nanoparticles, and their various applications. *Journal of Hazardous Materials Advances*, Vol. 13, 2024, id. 100401.

[2] Dhiman, V. and N. Kondal. ZnO Nanoadsorbents: A potent material for removal of heavy metal ions from wastewater. *Colloid and Interface Science Communications*, Vol. 41, 2021, id. 100380.
[3] Umadevi, G. and K. G. Krishna. Camellia sinensis-mediated green synthesis of ZnO nanoparticles: An eco-friendly approach for high-performance gas sensing. *Sensors and Actuators A: Physical*, Vol. 374, 2024, id. 115479.
[4] Antonette, L. C., N. R. Chandralekha, and J. Shanthi. Enhanced photodegradation of textile dye wastewater using silane/polymer doped ZnO nanocomposites and antibacterial activity. *Journal of the Indian Chemical Society*, Vol. 101, No. 10, 2024, id. 101254.
[5] Shakib, P., S. Z. Mirzaei, H. E. Lashgarian, R. Saki, G. Goudarzi, S. Alsallameh, et al. Preparation of zinc oxide nanoparticles assisted by okra mucilage and evaluation of its biological activities. *Current Drug Discovery Technologies*, Vol. 20, No. 2, 2023, id. e011222211472.
[6] Mirzania, F., I. Salimikia, Y. J. Ghasemian, A. Marzban, A. Firouzi, A. Nazarzadeh, et al. Biological activities of zinc oxide nanoparticles green synthesized using the aqueous extract of Dracocephalum kotschyi Boiss. *Current Drug Discovery Technologies*, Vol. 21, No. 4, 2024, id. e271223224899.
[7] Vandhana, T., T. Sandhiya, and A. J. C. Lourduraj. In vitro study of antibacterial and anticancer activities of biosynthesized Ag-doped ZnO nanoparticles from Anisochilus carnosus, Nephelium lappaceum, Calotropis gigantea. *Journal of Molecular Structure*, Vol. 1323, 2025, id. 140750.
[8] Ullah, S., M. Shaban, A. B. Siddique, A. Zulfiqar, N. S. Lali, M. Naeem-ul-Hassan, et al. Greenly synthesized zinc oxide nanoparticles: An efficient, cost-effective catalyst for dehydrogenation of formic acid and with improved antioxidant and phyto-toxic properties. *Journal of Environmental Chemical Engineering*, Vol. 12, No. 5, 2024, id. 113350.
[9] Cheraghipour, K., A. K. Khalaf, K. Moradpour, M. Zivdari, M. Beiranvand, P. Shakib, et al. Synthesis, characterization, and antiparasitic effects of zinc oxide nanoparticles-eugenol nanosuspension against Toxoplasma gondii infection. *Heliyon*, Vol. 9, No. 8, 2023, id. e19295.
[10] Ragavendran, C., C. Kamaraj, K. Jothimani, A. Priyadharsan, D. A. Kumar, D. Natarajan, et al. Eco-friendly approach for ZnO nanoparticles synthesis and evaluation of its possible antimicrobial, larvicidal and photocatalytic applications. *Sustainable Materials and Technologies*, Vol. 36, 2023, id. e00597.
[11] Abdelsattar, A. S., A. G. Kamel, M. A. Eita, Y. Elbermawy, and A. El-Shibiny. The cytotoxic potency of green synthesis of zinc oxide nanoparticles (ZnO-NPs) using Origanum majorana. *Materials Letters*, Vol. 367, 2024, id. 136654.
[12] Abegunde, S. M., M. A. Adebayo, and E. F. Olasehinde. Green synthesis of ZnO nanoparticles and its application for methyl green dye adsorption. *Green Energy and Resources*, Vol. 2, No. 2, 2024, id. 100073.
[13] Chandan, A. K., G. N. Mallika, and T. B. Narsaiah. A green approach to arsenic removal using ZnO nanoparticles synthesized from Acacia catechu leaf extract. *Materials Today: Proceedings*, Vol. 72, No. 1, 2023, pp. 110–119.
[14] Tharayil, J. M. and P. Chinnaiyan. Biogenic synthesis of ZnO from Rubia cordifolia root extract: A study on sono-photocatalytic dye degradation and anti-bacterial assay. *Results in Engineering*, Vol. 20, 2023, id. 101567.
[15] Sadiq, H., F. Sher, S. Sehar, E. C. Lima, S. Zhang, H. M. N. Iqbal, et al. Green synthesis of ZnO nanoparticles from Syzygium cumini leaves extract with robust photocatalysis applications. *Journal of Molecular Liquids*, Vol. 335, 2021, id. 116567.
[16] Hammam, M. A., S. A. El-Kadousy, S. M. El-Sayed, and R. M. Rashed. Hypolipidemic effect of Jamun Syzygium cumini. *Menoufia Journal of Agricultural Biotechnology*, Vol. 4, 2019, pp. 61–72.
[17] Driscoll, C. T. Acid and mercury deposition effects on forest and freshwater aquatic ecosystems. In: *Encyclopedia of biodiversity*, 3rd ed., Academic Press, New York, 2024, pp. 351–368.
[18] Zaman, Y., M. Z. Ishaque, S. Ajmal, M. Shahzad, A. B. Siddique, M. U. Hameed, et al. Tamed synthesis of AgNPs for photodegradation and anti-bacterial activity: Effect of size and morphology. *Inorganic Chemistry Communications*, Vol. 150, 2023, id. 110523.
[19] Siddique, A. B., D. Amr, A. Abbas, L. Zohra, M. I. Irfan, A. Alhoshani, et al. Synthesis of hydroxyethylcellulose phthalate-modified silver nanoparticles and their multifunctional applications as an efficient antibacterial, photocatalytic and mercury-selective sensing agent. *International Journal of Biological Macromolecules*, Vol. 256, No. Pt 1, 2024, id. 128009.
[20] Rajiv, P., S. Rajeshwari, and R. Venckatesh. Bio-Fabrication of zinc oxide nanoparticles using leaf extract of Parthenium hysterophorus L. and its size-dependent antifungal activity against plant fungal pathogens. *Spectrochimica Acta Part A: Molecular and Biomolecular Spectroscopy*, Vol. 112, 2013, pp. 384–387.
[21] Elumalai, K. and S. Velmurugan. Green synthesis, characterization and antimicrobial activities of zinc oxide nanoparticles from the leaf extract of Azadirachta indica (L.). *Applied Surface Science*, Vol. 345, 2015, pp. 329–336.
[22] Schuler, M. J., T. S. Hofer, Y. Morisawa, Y. Futami, C. W. Huck, and Y. Ozaki. Solvation effects on wavenumbers and absorption intensities of the OH-stretch vibration in phenolic compounds – electrical- and mechanical anharmonicity via a combined DFT/Numerov approach. *Physical Chemistry Chemical Physics*, Vol. 22, 2020, pp. 13017–13029.
[23] Anandan, M., S. Dinesh, N. Krishnakumar, and K. Balamurugan. Tuning the crystalline size of template free hexagonal ZnO nanoparticles via precipitation synthesis towards enhanced photocatalytic performance. *Journal of Materials Science: Materials in Electronics*, Vol. 28, No. 3, 2017, pp. 2574–2585.
[24] Rambabu, K., G. Bharath, F. Banat, and P. L. Show. Green synthesis of zinc oxide nanoparticles using Phoenix dactylifera waste as bioreductant for effective dye degradation and antibacterial performance in wastewater treatment. *Journal of Hazardous Materials*, Vol. 402, 2021, id. 123560.
[25] Saha, R., K. Subramani, S. Sikdar, K. Fatma, and S. Rangaraj. Effects of processing parameters on green synthesised ZnO nanoparticles using stem extract of Swertia chirayita. *Biocatalysis and Agricultural Biotechnology*, Vol. 33, 2021, id. 101968.
[26] Chennimalai, M., V. Vijayalakshmi, T. S. Senthil, and N. Sivakumar. One-step green synthesis of ZnO nanoparticles using Opuntia humifusa fruit extract and their antibacterial activities. *Materials Today: Proceedings*, Vol. 47, No. 9, 2021, pp. 1842–1846.
[27] Diallo, A., B. D. Ngom, E. Park, and M. Maaza. Green synthesis of ZnO nanoparticles by Aspalathus linearis: Structural & optical properties. *Journal of Alloys and Compounds*, Vol. 646, 2015, pp. 425–430.
[28] Elakkiya, G. T., G. Sundararajan, R. Lakshmipathy, P. Anitha, and N. Muruganantham. Prolific application of green synthesized CdS nanoparticles for the sequestration of cationic dyes from aqueous solution. *Bulletin of the Chemical Society of Ethiopia*, Vol. 38, No. 3, 2024, pp. 631–645.

[29] Alangari, A., M. A. M. Aboul-Soud, M. S. Alqahtani, M. Shahid, R. Syed, R. Lakshmipathy, et al. Green synthesis of Copper oxide nanoparticles using Inula genus and evaluation of biological therapeutics and environmental applications. *Nanotechnology Reviews*, Vol. 13, No. 1, 2024, pp. 1–15.

[30] Habib, A. K. M. A., K. M. R. Rifat, M. E. Kabir, J. N. Khan, S. M. N. Rokon, and M. A. Rabbi. Improved photocatalytic activity of (Ni, Mn) co-doped ZnO nanoparticles prepared via green synthesis route using orange peel extract. *Results in Materials*, Vol. 22, 2024, id. 100581.

[31] Thankachan, M. K., S. Ganapaty, D. Thomas, R. Chandrasekaran, S. K. Ramachandran, and M. Krishnan. Green fused nanoparticles from seaweed as a sustainable resource: Study on antimicrobial activities against human pathogens and photocatalytic degradation of methylene blue (MB) dye. *Inorganic Chemistry Communications*, Vol. 170, No. 3, 2024, id. 113415.

[32] Ahmad, A., A. N. Siyal, A. Elçi, and N. H. Kalwar. Ziziphus nummularia leaves extract mediated CuO nanostructures for photocatalytic degradation of Methylene Blue. *Desalination and Water Treatment*, Vol. 320, 2024, id. 100667.

[33] Qi, S., X. Hu, K. Zhang, H. Li, and S. Wu. Investigation of the mechanism and stability of highly efficient photocatalytic degradation of Methylene blue using Ni doped CdS photocatalyst. *Polyhedron*, Vol. 262, 2024, id. 117176.

[34] Jerin, I., M. A. Rahman, A. H. Khan, and M. M. Hossain. Photocatalytic degradation of methylene blue under visible light using carbon-doped titanium dioxide as photocatalyst. *Desalination and Water Treatment*, Vol. 320, 2024, id. 100711.

[35] Cheema, A. N., I. Muneer, F. Yasmeen, and D. Ali. Impact of niobium doping on photocatalytic degradation efficiency of iron oxide nanoparticles for methylene blue dye under UV and sunlight. *Materials Science and Engineering: B*, Vol. 312, 2025, id. 117878.

[36] Sirelkhatim, A., S. Mahmud, A. Seeni, N. H. M. Kaus, L. C. Ann, S. K. M. Bakhori, et al. Review on zinc oxide nanoparticles: antibacterial activity and toxicity mechanism. *Nano-Micro Letters*, Vol. 7, 2015, pp. 219–242.

[37] Zamana, Y., M. Z. Ishaquea, R. Sattarb, M. M. Rehmanb, I. Sabac, S. Kanwala, et al. Antibacterial potential of silver nanoparticles synthesized using tri-sodium citrate via controlled exploitation of temperature. *Digest Journal of Nanomaterials and Biostructures*, Vol. 17, No. 3, 2022, pp. 979–987.